Desalination and Water Treatment
www.deswater.com

doi: 10.5004/dwt.2022.28957

277 (2022) 62–71
November

Evaluation of bisphenol A pollutant removal efficiency by nano photocatalytic method in solar reactor (UV_A and CPC) and reactor UV_C

Z. Zanganeh[a], Ayat Rahmani[a], Yousef Dadban Shahamat[b], Hamidreza Nassehinia[a,*]

[a]*Department of Environmental Health Engineering, Semnan University of Medical Sciences, Semnan, Iran, email: hrnassehi@semums.ac.ir (H. Nassehinia)*
[b]*Department of Environmental Health Engineering, Gorgan University of Medical Sciences, Gorgan, Iran*

Received 6 April 2022; Accepted 25 September 2022

ABSTRACT

Bisphenol A (BPA) and its derivatives have extensive applications as lubricants and polymer stabilizers and components of photographic developers. In this study, the photo catalytic degradation of bisphenol A (BPA) was studied on ZnO nanoparticles coated on a fixed bed which was treated in two light sources including ultraviolet-C (UV_C-254 nm) and natural solar in compound parabolic concentrators (CPC). Characterization of the ZnO nanoparticles samples was performed by field-emission scanning electron microscope, X-ray diffraction, ultraviolet-visible (UV-VIS) spectrophotometer, and Brunauer–Emmett–Teller measurements. The highest photocatalytic and photolysis activity for the degradation of BPA has been obtained for the ZnO/UV_C and UV_C with 99% and 40% efficiencies in 120 min. Also, the highest photocatalytic and photolysis activity for the degradation of BPA has been obtained for the CPC reactor and 97% and 31% efficiency in 120 min. The photocatalytic degradation reaction of BPA was monitored by high-performance liquid chromatography, total organic carbon, and gas chromatography/mass (GC-MASS) analyses. The results of GC-MASS analysis show that the degradation of BPA occurs through the production of glycolic acid, benzoic acid, and vinyl phenol products and its decomposition occurs by ring fission and then subsequent reactions with OH radicals. These results show that the photo catalytic degradation of solar light and UV has high efficiency in BPA removal as well as effluent mineralization.

Keywords: Zinc oxide (ZnO); Photocatalyst; Ultraviolet-c (UV_C); Compound parabolic concentrators (CPCs); Bisphenol A (BPA)

1. Introduction

Endocrine-disrupting compound (EDC) is an exogenous substance or a mixture that alters the function(s) of the endocrine systems and consequently causes adverse health effects in an intact organism [1]. Such compounds include phthalates, bisphenols, pesticides, polychlorinated biphenyls, polycyclic aromatic hydrocarbons, and heavy metals [2]. In recent years, bisphenol A (BPA) with chemical formula 2,2-bis(4-hydroxyphenyl)propane or 4,40-isopropylidenediphenol [3], one of the most typical EDCs, has been proven to be a huge threat to human health and the environment even at trace levels [4]. BPA can be detected in water and wastewater and its concentration varies considerably (from ng/L to μg/L) [5]. BPA is a synthetic chemical with wide-spread applications in the production of polycarbonate plastics and epoxy resins [6] that are used in microwave ovenware, food containers, medical devices and personal care products, among other uses. The purpose of adding BPA to polycarbonate is to increase the durability of the plastic [7–9]. The global BPA market is expected to reach around 7,348 thousand tons by the end of 2023 [10]. Therefore, highly efficient and stable methods are urgently needed to remove BPA from water

* Corresponding author.

environments. The methods for EDC removal from water can be classified into three categories: physical removal, biological treatment and advanced oxidation processes (AOPs) [11]. Some of the common treatment approaches such as activated carbon adsorption are restricted due to the low hydrophobicity ($\log K_{OW}$ = 3.32) of BPA that limits its adsorption [12]. Further, due to its very low Henry's constant (1×10^{-10} at 25°C), air stripping is not generally feasible due to the requirement for a high air-to-water ratio which increases the cost of treatment [13].

The efficiency and simplicity of AOPs make them a suitable choice for the removal of toxic chemicals from wastewaters in the recent years [14]. Hence, AOPs appear appropriate alternatives for the degradation and mineralization of BPA in water and wastewater [15]. Several AOPs have been utilized for the generating of •OH, including Fenton processes, photolysis, ozonation, photocatalysis, water solution treatment by electronic or γ beams and various combinations of these methods [16–18]. The disadvantages of ozonation alone (O_3 system) in treating wastewater include high energy cost of its generation and slow reaction rate [19]. The Fenton system is attractive because of its very fast reaction rates, low toxicity, and simplicity to control [20]. However, Fenton and Fenton-related processes have some intrinsic drawbacks, such as high H_2O_2 dosage, strict pH range and the accumulation of ferric oxide sludge, which cause a decrease in the oxidation rate [21,22]. In recent decades, using semiconductor based (heterogeneous) photocatalysis as the most effective AOPs could overcome to these disadvantages [23]. Photocatalytic processes have many advantages for treatment of contaminated water including the complete oxidation of organic pollutants, availability of high activity catalysts, being inexpensive and compatible with a particular design of reactor systems [24]. In this cost effective process, the attacks of the radicals and the e/h pairs to the pollutant molecules convert them into the smaller intermediates and finally into carbon dioxide, water, and other inorganic species [25–27]. The photocatalytic properties of numerous semiconductors have been investigated (TiO_2, ZnO, Fe_2O_3, V_2O_5, WO_3) [28,29]. Between these, the most commonly used for water treatment applications are titanium dioxide (TiO_2) and zinc oxide (ZnO) [30]. Zinc oxide nanoparticles (ZnO-NPS) have attracted much attention in nanotechnology research among other metal oxides due to non-toxic, non-hygroscopic metal oxide with high photosensitivity, mainly in the degradation of various pollutants. ZnO has higher photocatalytic activity than TiO_2 in some conditions. The biggest advantage of ZnO in comparison with TiO_2 is that it absorbs over a larger fraction of UV spectrum [31,32]. In addition to small scale studies, several pilot plant experiments have been performed in order to test the applicability of solar photocatalysis for wastewater treatment. One of the best options of reactors for photocatalytic applications using sunlight is the compound parabolic concentrators (CPC) reactors [33,34]. CPCs are the static solar collectors that concentrate all of the incident solar radiation below a certain angle so that the radiation reflected by the surface of the collectors also reaches the lower part of the reactor and the entire surface is irradiated almost homogeneously [35,36]. The advantages of CPC reactors are: the possibility of using solar UV radiation coming from all directions in the sky (global UV radiation), simplicity of construction and operation, turbulent flow regime (which improves mass transfer), and high reduction of the vaporization of volatile pollutants [33,34].

The use of a new structure in the simultaneous use of photocatalyst and Sunlight in order to degradation and mineralization of BPA without adding any chemicals and energy consumption is novelty and one of the main objectives of this project.

The purpose of this study has been to assess the feasibility of the photocatalytic degradation of bisphenol A in the presence of ZnO nanoparticles coated on the fixed bed and two light sources, ultraviolet-c (UV_C-254 nm), and solar light.

2. Experimental

Bisphenol A (purity 99%) was obtained from Sigma-Aldrich and the stock solutions for BPA (100 mg) were freshly prepared by dissolving a suitable number of solid reagents with deionized water (DI water). Other materials used in the experiments, including zinc oxide (ZnO 99.8%), fluoride acid, acetonitrile, and water grade high-performance liquid chromatography (HPLC) were purchased from Merck, Germany.

2.1. Preparation of ZnO

First, to create a higher effective surface on the glass, the glass surface was placed in contact with 30% fluoride acid for 50 min. The glass beds were washed with distilled water and then they were set in plastic containers containing NaOH 1 normally for 50 min. For making the ZnO solution, the ZnO powder with 99.8% purity was prepared and the solution with 3% ZnO was made. In the next step, the solution is placed in an ultrasonic apparatus at 50°C for 90 min to obtain a homogeneous mixture. After distributing this homogeneous suspension on the glass surface, it was placed at a normal temperature for 3–4 h. After this period of time, the amount of water remaining on the residual glass surface was removed and the sample was placed at a normal temperature for 24 h to dry again. After this step, the glass was placed in the furnace for 1 h and a half and the temperature gradually increased from 50°C to 500°C to create the calcification of the nanoparticles on the substrate surface.

2.2. Construction of the reactor

In this research, three kinds of reactors (Reactor 1 (CPC), Reactor 2 (UV_C 250 nm), and Reactor 3 (solar)) were used.

In this study, one sort of the reactor CPC was used. The reactor applied in this research (CPC) has a reflect surface with the width of 100 cm and the length of 150 cm, which is able to reflect more sunshine to a reactor focal point (Fig. 1b). In this research, the reflective surface of CPC was used, including a mirror with a width of 2 mm, which reflected 86% of ultraviolet rays and 96% of other solar rays. [36]. A quartz tube was placed at a distance of 7.5 cm from the mirror at the focal point of the reactor. The quartz glass tube applied in Reactor 1 had measurements of 150 cm width, 5 cm external diameter, and 1.5 mm wall thickness and 2.95 L

inner volume, Fig. 1a. The glass tubes can spread 94% and 54% of UV_A and UV_B light, separately [37]. In this research, an aluminum metal with a black color was used as a superconductor which was capable to speed up and increasing the rate of warm for removal BPA (Fig. 1c). Pyrex glasses containing ZnO coated on a metal rod 100 cm long, 3 cm wide, and 1 mm thick, which was painted with black spray paint, were placed at regular intervals with the help of glue and placed inside the quartz tube [37].

Reactor 2 (UV_C reactor) was used for direct use of UV_C rays, and Reactor 3 (UV_A) was used to use sunlight without focusing light. In the glass, Reactor 2 was designed (30 cm × 16 cm × 20 cm) ،then a glass bed coated with ZnO was placed at the bottom of the reactor. The light source in Reactor 2 was an UV_C lamp with an average pressure and a nominal power of 8 W/h and a length of 30 cm, which is placed exactly in the center of a mirror cylinder used as the reactor cap. Reactor 3 with the same design was used and solar light was used as a light source in the photo catalytic process (Fig. 2).

2.3. Characterization techniques

In order to investigate the physical and chemical properties of materials, scanning electron microscope (SEM) and X-ray diffraction (XRD) were done [38].

2.4. Experiments

In this study, a stoke 100 mg/L powder of bisphenol A was used to prepare the test solutions. The time period of study in this research was (120, 90, 60, 45, 30, 15, 10, 5, and 0 min). HPLC was used to measure residual concentrations in wastewater. The solutions were prepared as standard concentrations (1, 5, 10, 15 mg/L) from the stoke sample to obtain peak time and a calibration curve. Then, different concentrations of bisphenol A were prepared; a sample with a constant concentration of 10 mL with a volume of 1 L was added to the reactors. After sunlight emission and UV_C at a wavelength of 254 nm at specified times, the sample was transmitted to the HPLC apparatus for analysis. The bisphenol A concentration was measured by a standard HPLC apparatus with a C_{18} column and acetonitrile and water moving phase (55:44 v/v) [39].

2.5. Gas chromatography/mass analysis

In order to determine the degradation process of the contaminants and intermediate materials in the refined solution, the samples were analyzed on the gas chromatography/mass (GC-MASS) device. For preparation of the samples for testing, 10 cc from samples after irradiation times that were filtered with 1 cc chloroform and 4 cc acetonitrile, were mixed in a falcon tube, and placed in a centrifuge

Fig. 1. Reactor CPC.

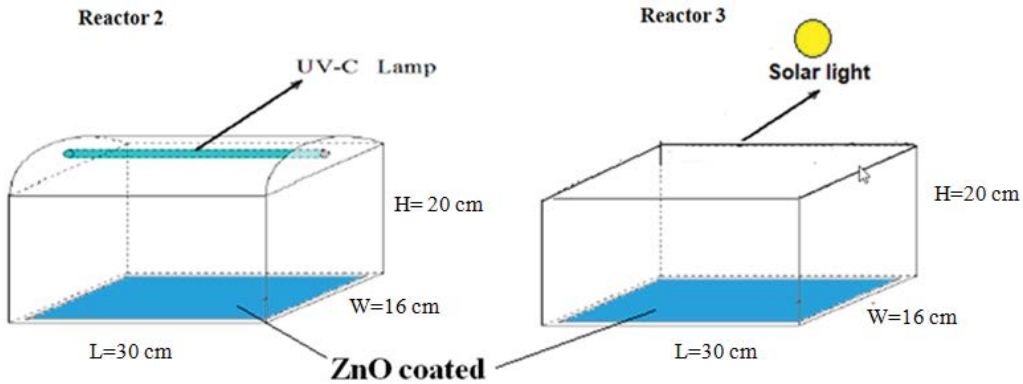

Fig. 2. Schematic of the Reactors 2 and 3 used in this study.

machine at 3,500 rpm for 30 min; then, 1 cc of the solution in the separated phase was taken from the surface and injected into the GC-MASS.

2.6. Reaction kinetics

In this study, Eq. (1) was used to calculate the reaction kinetics.

$$\ln\frac{C}{C_0} = -Kt \tag{1}$$

where C_0 is the initial concentration and C is the concentration of the wastewater. t is the solution contact time in the reactors and K is the reaction speed constant [40].

2.7. Solar experiment

All experiments were performed under natural solar radiation in Damghan-Iran, that geographical location was 54° 20′ 34.51″ E and latitude 36° 10′ 4.44″ N which had a very good position to use solar energy.

Tests started at 11 am and finished at 17 pm local time. Samples (10 mg /l BPA) were taken after 5, 10, 15, 30, 45, 60, 90 and 120 min of solar exposure and to ensure reproducibility of results, each sample was done three times. The reactor to the north–south and at an angle of 35° to 15° considering the region and the season were placed. Solar and UV irradiance was measured with a global UV radiometer (295–385 nm UV and 400–1,500 nm solar, Model HAGNER, Sweden). The primary temperature of all the samples was about 45°C ± 10°C.

2.8. Brunauer–Emmett–Teller

The effective surface of nanoparticles, in both powdered form and after coating conditions, has been determined by the Brunauer–Emmett–Teller (BET) machine. In this study, the ZnO sample was first prepared in powder form before coating, and then the nanoparticles after coating were prepared to test the effective surface area.

2.9. Total organic carbon test

The concentration of total organic carbon (TOC) was measured with a TOC analyzer (Jena-C3100 made in Germany). The TOC test was used to control the process of mineralization of the samples. For this purpose, 10 cc of the sample after the reaction time of 120 min was taken and after injecting 0.1 cc HCl 1 normal, the NPOC content of the sample was measured by the TOC Meter machine at 800°C furnace temperature.

The degree of BPA mineralization in the VU_C/ZnO process was determined by Eq. (2). Where TOC_0 and TOC_t represent the TOC concentrations (mg/L) in the solution at the beginning and time t [41].

$$\text{BPA mineralization}\ (\%) = \left(\frac{TOC_0 - TOC_t}{TOC_0}\right)\times 100 \tag{2}$$

3. Results and discussion

3.1. Characterization of the nanocatalyst

The surface morphology was characterized by scanning electron microscopy (SEM). In Fig. 3a, field-emission scanning electron microscope (FE-SEM) shows the surface of the glass substrate before coating. This provides the contact of the substrate with HF and corrosion on the glass surface, leading to providing a suitable substrate for the nanoparticle coating. Fig. 3b shows the substrate after coating that the nanoparticle has been uniformly distributed over the entire surface. Fig. 3c shows the size of the particles in the indicated layer. After the coating process, the size of the crystals is larger than the powdery state. During the coating process, the size of nanoparticle crystals has increased from 20 nm in a powdery state to 32 nm after the coating. Changes in the size of the nanoparticle crystal can be caused by the high calcification on the surface of the glass substrate [42]. Immobilization of nanoparticles and lack of change in the morphology of bed silica show the results of the operation of ZnO deposition.

3.2. XRD analysis

The results of the XRD of powdered nanoparticles and the layer coated on the glass substrate has been shown in Fig. 4. The photoactivity of ZnO depends on many parameters containing the crystal structure, the number of nanoparticles in anatase and rutile phases, particle

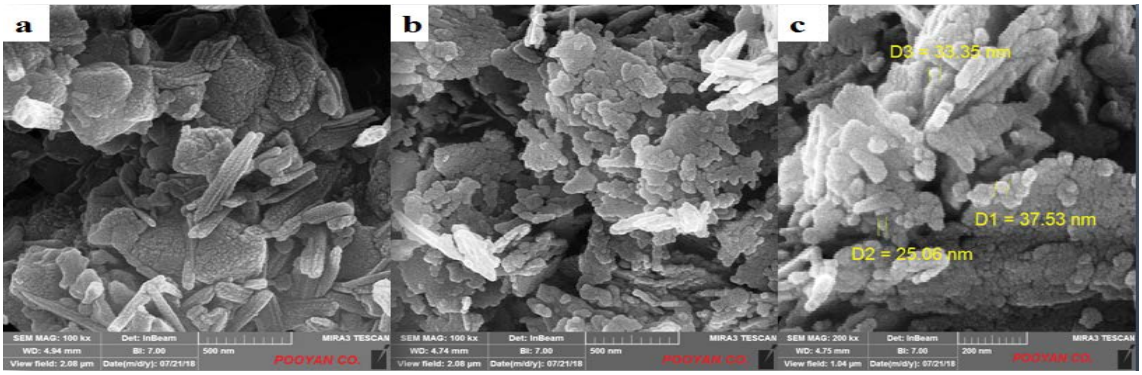

Fig. 3. FE-SEM surface of the glass substrate before coating (a), and after coating with ZnO (b,c).

dimensional distribution, specific surface area and means pore size. The microcrystal structure of the ZnO before and after coating was characterized with the X-ray diffracts meter (XRD) analysis. The XRD pattern of the pure catalyst and CDH binder catalyst coating has been displayed in Fig. 4a and b. Results displayed in Fig. 4a clearly show that there was basically no change in the X-ray diffraction pattern of ZnO [43,44].

XRD pattern of ZnO NPs agreed with that of hexagonal wurtzite zinc oxide crystallite phase (JCPDS pattern no 36-1451) because the ZnO-wurtzite showed typical diffraction peaks which positioned at 2θ values of 31.7° (1 0 0), 34.44° (0 0 2), 36.24° (1 0 1), 47.53° (1 0 2), 56.59° (1 1 0), 62.9° (1 0 3), 66.4° (2 0 0), 67.97° (1 1 2), and 69.12° (2 0 1) [45]. The peaks in the ZnO XRD pattern indicate the narrow size distribution of nanoparticles in the samples, implying that the diffraction peaks are almost strong. These results corroborated that the peak positions matched well with the standard data for bulk ZnO [46].

3.3. BET surface area

Due to the contact of HF with the surface of the substrate, corrosion and unevenness are created on the surface of the substrate. In this way, the surface of the substrate is an uneven surface and when the nanoparticle is coated on this substrate, according to the data of the device analysis; its effective surface is reduced by 3–4 m^2/g (approximately 10%–15%).

The results of the BET test show that during the coating process, the nanoparticle crystals have decreased from 50.1 m^2/g in a powdery state to 47.2 m^2/g after the coating. According to Ahmadi et al. [38], this reduction in size is the result of the calcification process during the coating process [38].

3.4. Solar light

The investigation was carried out on sunny days without cloud cover. Fig. 5 shows the peak sun hours of 11.30 to 14.30, so tests were done at the same time. The maximum IR and UV radiations in natural solar light were 700 and 37 W/m^2 (Fig. 5b) and the IR and UV radiation maximum in CPC were 7,000 and 160 W/m^2, respectively (Fig. 5a). Due to the geographical area of Damghan, where 1,054.6 h of solar light is in the summer, the use of solar light for removal efficiency of bisphenol A contaminant from synthetic aqueous solution can be considerable.

3.5. Photolysis degradation of BPA

First, to examine the rate of the BPA photolysis, experiments were conducted with three reactors, Reactor 1 (CPC) , Reactor 2 (UV_C 250 nm) and Reactor 3 (solar light). Fig. 6 shows the photodegradation of BPA in different reactors. The result showed that the highest rate of photolysis in Reactor 2 is 43% after 120 min UV irradiation and the maximum absorption of UV is at wavelengths of 245 nm by

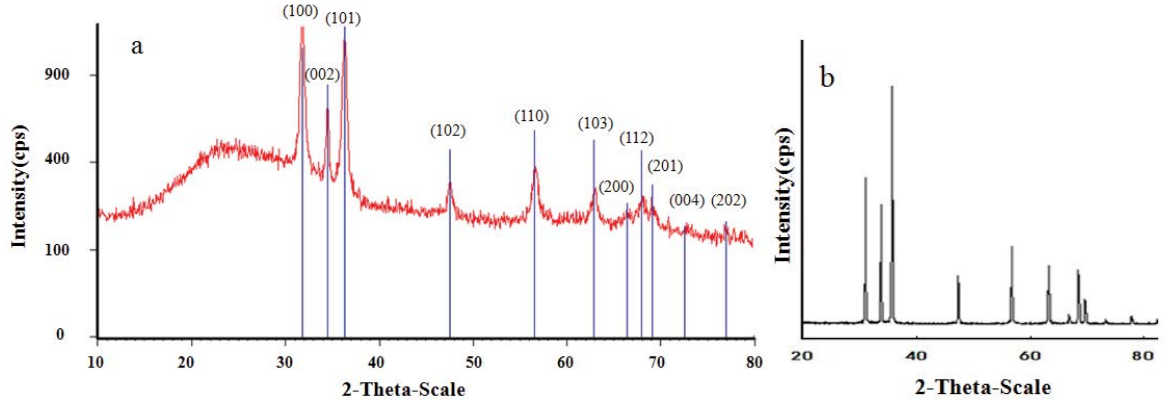

Fig. 4. XRD for ZnO samples after coating (a), and before coating (b).

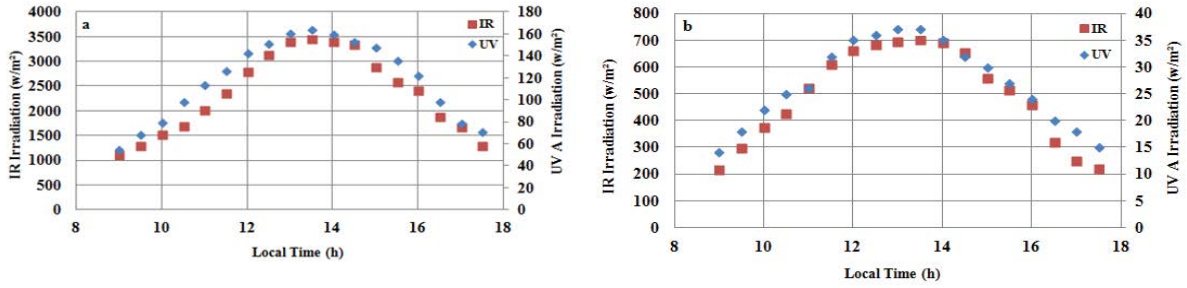

Fig. 5. Graphic representations of the values of solar UV and solar irradiance radiations registered during the degradation, CPC (a) and solar (b).

bisphenol A [47]. The amount of the bisphenol A is broken down and converted to by-product materials. The effect of sunlight on solar Reactor 1 is 31% with irradiance 3,456 and UV_A 164 W/m^2 and in Reactor 3 it is 12% with irradiance 700 and UV_A 37 W/m^2. The UV type and intensity caused this result. On the other hand, the amount of UV absorption by bisphenol A is negligible at wavelengths over 365 nm, which can prevent the degradation of bisphenol A by sunlight over short periods of time [48].

By the study of Kang et al. showed that BPA was hardly degraded under UV_A and UV_B light. More intermediates can be exited during UV_C photolysis, and can attack the mother compound as described by Eq. (3) [47].

$$\text{Intermediates} + hv \rightarrow \text{Intermediates} + \text{BPA} \rightarrow \text{Products} \quad (3)$$

The range of wavelengths of the sun's energy passes through the water, the absorption rate was low and the majority of the light passes through water [49]. That's why, to use the solar visible light wavelength in the range of 300–1600 nm, we used a black aluminum metal which was a strong absorbent of solar visible light in Reactor 1 (CPC) [37].

3.6. Photo catalytic degradation of BPA

In this study, the photocatalytic degradation of bisphenol A was studied on the ZnO nanoparticles coated fixed bed, which was treated in three reactors, Reactor 1 (CPC), rector 2 (UV_C 250 nm) and Reactor 3 (solar light). To determine the concentration of bisphenol A by HPLC, the standard concentrations (1–15 mg/L) were injected into the device and the chromatogram peaks of biphenyl a formed at a retention time of 2.947 min were registered. Calibration curves have been shown in Fig. 7a and b. After this step, the test samples were injected into HPLC to determine the remaining concentration.

The efficiency of contaminant removal in Reactor 2 was 80% after 30 min and 99% after 120 min, while solar Reactors 1 and 3 had an elimination efficiency of 73% and 40% at 30 min respectively (Fig. 8). Solar driven AOPs should have a lower cost and may be applied to the sustainable treatment of drinking water and irrigation water. ZnO photocatalysis has attracted great interest due to its high efficiency for OH• generation [37]. The ZnO has a 3.2 eV band gap and is excited by radiation within 200–400 nm wavelength. This material shows the highest absorption in the range of 360–385 nm [50].

The most important factor in the degradation of bisphenol A is the presence of free radicals of OH• resulting from the photocatalytic process. The increased contact area between the deposited adsorbent and the contaminant, enumeration of active sites, and production of free electrons in the conductive band are the reasons for elevation of removal efficiency by increasing the nano photocatalyst mass. The photo decomposition rate of the organic pollutant is influenced by the number of active sites as well as the light absorption ability of the photocatalyst. For a suitable high concentration of the catalyst, the degradation occurs

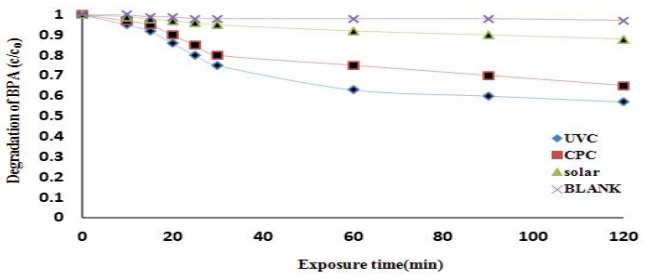

Fig. 6. Effect of solar, CPC and UV_C on photolysis degradation of BPA.

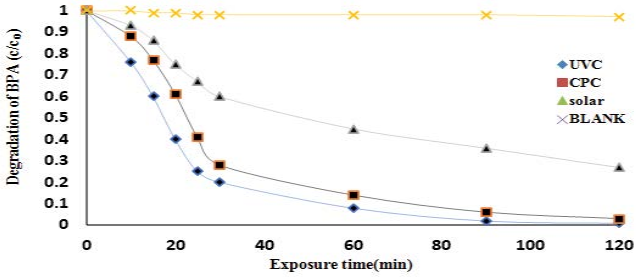

Fig. 8. Effect of solar, CPC and UV_C on photocatalysis degradation of BPA.

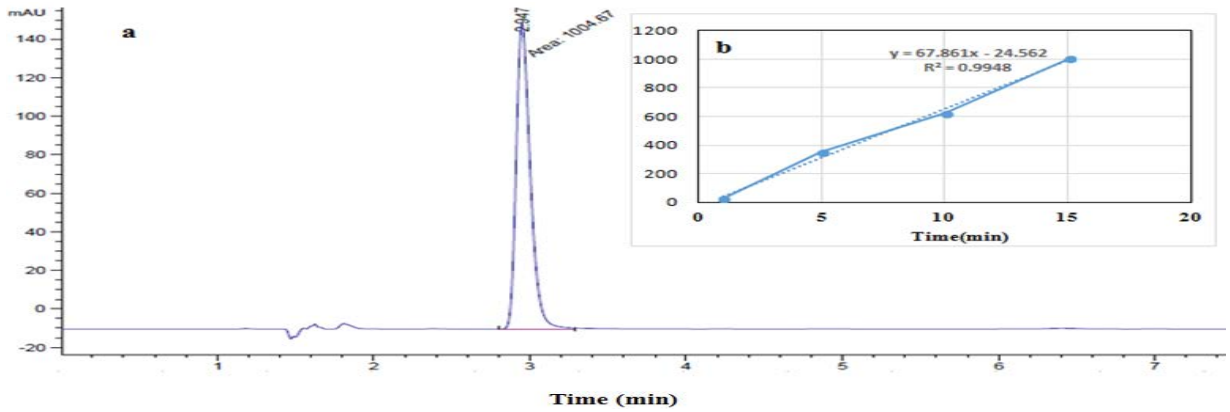

Fig. 7. Chromatogram peaks of BPA (a) and calibration curves (b).

rapidly because of generating more hvb + and ecb [51]. In conclusion, it can be said that Reactor 2 is capable of producing more free radicals, resulting in higher efficiency in bisphenol A removal. Comparing two solar reactors, the CPC reactor, which is a light concentrator, has higher efficiency and efficiency than Reactor 3, which is a conventional solar reactor. The reason for this difference is two factors: intensity of light irradiation and temperature rise. As shown in Fig. 5, the intensity of IR and UV_A in the CPC are irradiance of 3,456 and 164 W/m^2, respectively. In the solar reactor, 700 and 37 W/m^2, respectively. Therefore, according to previous studies, the increase in the intensity of light radiation increases the efficiency of the photocatalytic process and the production of free radicals that are effective in removing bisphenol A [52,53]. The reason for reducing the degradation efficiency in solar reactors like Reactor 2 can be related to a reduction of light absorption at wavelengths more than 385 nm on the catalyst surface, as well as the reduction of the sun's UV intensity to the UV produced by the 18-W argon lamp [54]. On the other hand, it is generally accepted that temperature is a critical parameter determining the photocatalytic reaction rate [55]. Temperature exerts an insignificant enhancement on BPA degradation due to the high speed of photocatalytic degradation [56].

3.7. Kinetic

Photolysis in 254 nm and OH• oxidation are two mechanisms that contributed to the degradation of BPA [57]. Fig. 9 shows the kinetic reaction of biphenyl A. It can be seen that the kinetic reaction of photolysis in biphenyl a solution, which is contacted with a UV lamp (254), is 3.6 × 10^{-3} in 30 min. The kinetic reactions in photocatalytic process in Reactor 1, Reactor 2, and Reactor 3 are 53.647 × 10^{-3}, 109.894 × 10^{-3}, and 17.027 × 10^{-3}, respectively, in 30 min. Overall, the reason for increasing the reaction rate in Reactor 2 is due to production of higher OH• radical than other reactors. The reaction speed of Reactors 1 and 3, which use solar radiation at wavelengths of more than 300 nm, as solar source in the photocatalytic process, is lower than Reactor 2. The main reason for this difference is that the most absorbing light ZnO is at 254 nm wavelength and it has a lower light absorption at the wavelength of the sunlight, resulting in a lower free radical of OH• in Reactors 1and 3. The kinetic reaction of the CPC reactor (53.647 × 10^{-3}) is greater than the ordinary solar reactor (17.027 × 10^{-3}). The intensity of the UV rays in Reactor 1 goes up (162 W/m^2) because of the structure of the CPC in comparison with the intensity of UV Reactor 3 (34.4 W/m^2) so that this rise could be boost free radical production [37].

3.8. TOC analysis

Complete mineralization of BPA is of great importance in water and wastewater care processes [56]. The effectiveness of the oxidation/mineralization of an organic combination is determined through the removal of overall TOC from the wastewater [58]. Therefore, TOC removal was used to assess the mineralization extent of BPA throughout the photo catalytic reaction. The consequences of the TOC degradation effectiveness of BPA in improved situations have been exposed in Fig. 10. The BPA under improved circumstances shows great efficiency and nearly fully degraded after 120 min. Also, the total TOC removal proves a similar trend, but the rate is a tiny bit slower [56]. The quantity of the TOC degradation efficacy started from 3% in 5 min, reaching 77% in 90 min and reaching 81% at the end of the 120 min. The minor rate of BPA mineralization rather than that of its degradation can be connected to the creation of organic middles simpler than BPA in arrangement through the degradation methods [59]. Later on, these intermediates are degraded and BPA mineralized after 120 min [42].

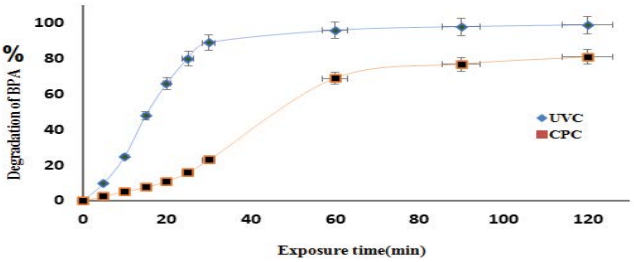

Fig. 10. TOC degradation efficiency of BPA at optimized conditions.

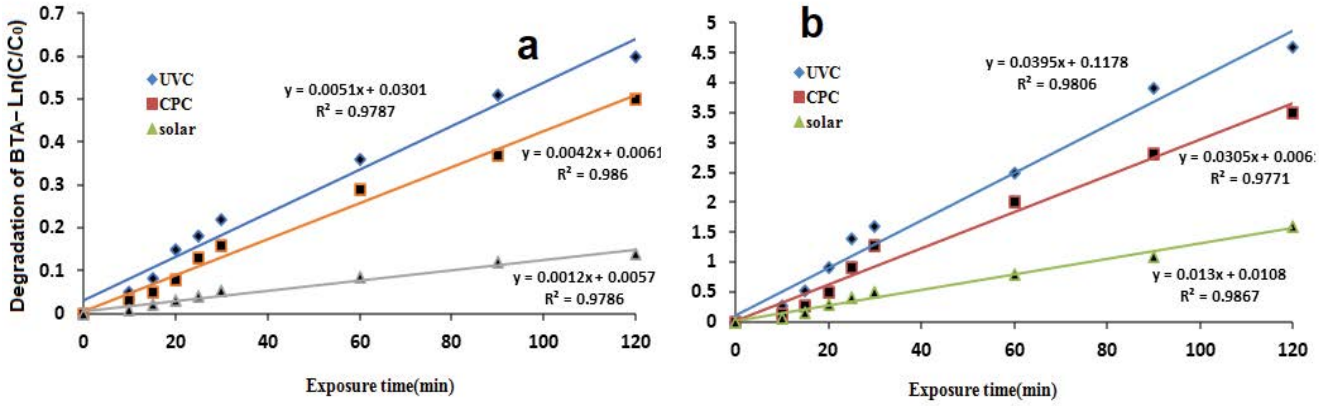

Fig. 9. Reaction kinetics of BPA in photolysis (a) and photocatalytic (b) degradation.

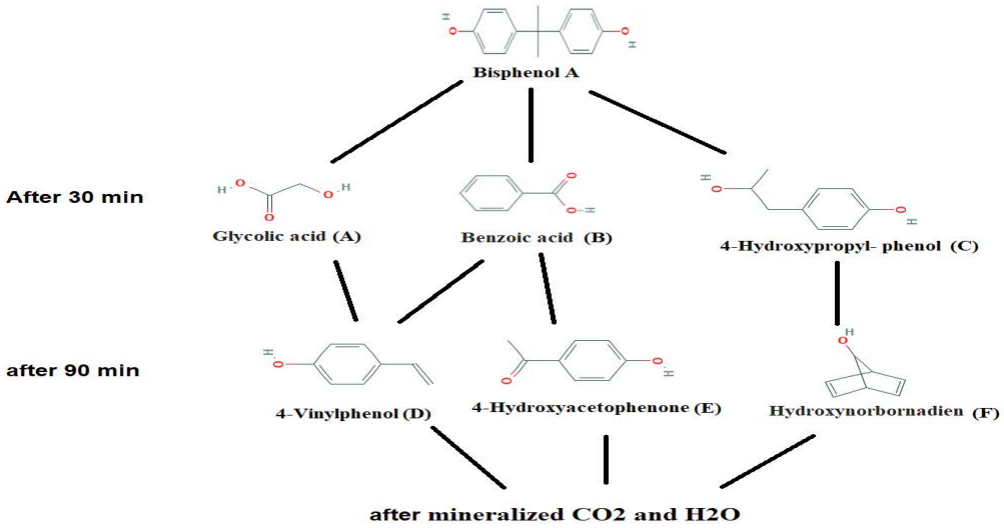

Fig. 11. Mass spectra data of the intermediates from decomposed BPA by GC-MASS.

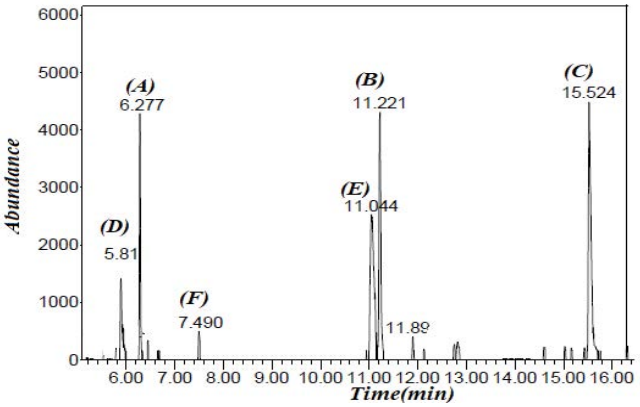

Fig. 12. GC-MASS chromatogram of the degradation of bisphenol A.

A decrease in the TOC value and an increase in the inorganic carbon (IC) value imply that the degradation of BPA results in the opening of the aromatic ring and the formation of inorganic acids [58].This explains that photo catalytic oxidation has an great benefit in its random strong oxidation capability, which can rot pollutants into not hurtful CO_2 and H_2O quickly and securely [56].

3.9. GC-MASS analysis

In the GC-MASS test, samples of the reactors were extracted at 30- and 90-min times. Compounds that were possibly created by the degradation of bisphenol A and indicated by the GC-MASS test in Fig. 11 (molecular structure) and Fig. 12 (GC-MASS chromatogram) and from A to F were numbered respectively. The structure of bisphenol A is based on two unsaturated phenol rings [60]. Generally, the BPA photocatalytic degradation is believed to be initiated through attacks by $OH^{\bullet}$ at the electron-rich C_3 in the phenyl group of BPA. Products after 30 min exposure, free radicals created in the photo catalytic process like $OH^{\bullet}$ and $O^{\bullet}$ can cause breaking structures between the C–H and O–C bonds. As shown in Fig. 11, in the first reaction, after breaking down the contaminant's structure, materials such as benzoic acid, glycolic Acid and 4-hydroxypropyl-phenol, whose structure has been shown in Fig. 11 (Product A to C). After 90 min, the materials in contact with free radicals are broken down and form a simpler material whose structure has been shown in Fig. 11 (Product D to F). All these intermediates are eventually mineralized into CO_2 and H_2O by sequentially photo catalytic processes [61,62].

4. Conclusion

It can be said that a ZnO nanoparticle bed can produce a catalytic surface for the photocatalytic process with a coating on the glass substrate. Both natural and artificial UV light sources are capable of generating electrons and cavities at the catalyst surface and then creating free radicals such as $OH^{\bullet}$. Free radicals initially show a high tendency to react with the molecular structure of bisphenol A and turn it into a circular intermediate substance, and then the loops open, turning into simpler structures. Ultimately, in the vicinity of OH·, these materials convert to CO_2 and H_2O.

Acknowledgements

This paper is a result of a research plan with the number of 1402 at Semnan University of Medical Sciences and it has been conducted with the financial support of the research and technology administration of the University. Hereby, their support and help are highly acknowledged.

References

[1] R.T. Zoeller, T.R. Brown, L.L. Doan, A.C. Gore, N.E. Skakkebaek, A.M. Soto, T.J. Woodruff, F.S. Vom Saal, Endocrine-disrupting chemicals and public health protection: a statement of principles from the endocrine society, Endocrinology, 153 (2012) 1422, doi: 10.1210/en.2012-1422.

[2] M.P. Fernandez, M.G. Ikonomou, I. Buchanan, An assessment of estrogenic organic contaminants in Canadian wastewaters, Sci. Total Environ., 373 (2007) 250–269.
[3] E.N. Bocharnikova, O.N. Tchaikovskaya, O.K. Bazyl, V.Y. Artyukhov, G.V. Mayer, Chapter Seven – Theoretical Study of Bisphenol A Photolysis, In: Advances in Quantum Chemistry, Vol. 81, 2020, pp. 191–217.
[4] L. Luo, Y. Yang, M. Xiao, L. Bian, B. Yuan, Y. Liu, F. Jiang, X. Pan, A novel biotemplated synthesis of TiO_2/wood charcoal composites for synergistic removal of bisphenol A by adsorption and photocatalytic degradation, Chem. Eng. J., 262 (2015) 1275–1283.
[5] H. Zhang, J. Shi, X. Liu, X. Zhan, Q. Chen, Occurrence and removal of free estrogens, conjugated estrogens, and bisphenol A in manure treatment facilities in East China, Water Res., 58 (2014) 248–257.
[6] M.H. Mahmoudian, A. Mesdaghinia, A.H. Mahvi, S. Nasseri, R. Nabizadeh, M.H. Dehghani, Photocatalytic degradation of bisphenol A from aqueous solution using bismuth ferric magnetic nanoparticle: synthesis, characterization and response surface methodology-central composite design modeling, J. Environ. Health. Sci. Eng., (2022), doi: 10.1007/s40201-021-00762-2.
[7] N. Mandel, B. Gamboa, M. Cebrián, Á. Mérida-Ortega, Challenges to regulate products containing bisphenol A: implications for policy, Salud. Publica. Mex., 61 (2019) 692–697.
[8] J.B. Hansen, N. Bilenberg, C.A.G. Timmermann, R.C. Jensen, H. Frederiksen, A.M. Andersson, H.B. Kyhl, T.K. Jensen, Prenatal exposure to bisphenol A and autistic- and ADHD-related symptoms in children aged 2 and 5 years from the Odense Child Cohort, Environ. Health., 20 (2021) 24, doi: 10.1186/s12940-021-00709-y.
[9] W. Ratajczak-Wrona, M. Garley, M. Rusak, K. Nowak, J. Czerniecki, K. Wolosewicz, M. Dabrowska, S. Wolczynski, P. Radziwon, E. Jablonska, Sex-dependent dysregulation of human neutrophil responses by bisphenol A, Environ. Health., 20 (2021) 5, doi: 10.1186/s12940-020-00686-8.
[10] I. Forner-Piquer, I. Fakriadis, C. Mylonas, F. Piscitelli, V. Di Marzo, F. Maradonna, J. Calduch-Giner, J. Pérez-Sánchez, O. Carnevali, Effects of dietary bisphenol A on the reproductive function of gilthead sea bream (*Sparus aurata*) testes, Int. J. Mol. Sci., 20 (2019) 5003, doi: 10.3390/ijms20205003.
[11] Z.-h. Liu, Y. Kanjo, S. Mizutani, Removal mechanisms for endocrine disrupting compounds (EDCs) in wastewater treatment—physical means, biodegradation, and chemical advanced oxidation: a review, Sci. Total Environ., 407 (2009) 731–748.
[12] K.J. Choi, S.G. Kim, C.W. Kim, J.K. Park, Removal efficiencies of endocrine disrupting chemicals by coagulation/flocculation, ozonation, powdered/granular activated carbon adsorption, and chlorination, Korean J. Chem. Eng., 23 (2006) 399–408.
[13] T. Garoma, S. Matsumoto, Ozonation of aqueous solution containing bisphenol A: effect of operational parameters, J. Hazard. Mater., 167 (2009) 1185–1191.
[14] A.N. Ejhieh, M. Khorsandi, Photodecolorization of Eriochrome Black T using NiS-P zeolite as a heterogeneous catalyst, J. Hazard. Mater., 176 (2010) 629–637.
[15] A. Cesaro, V. Belgiorno, Removal of endocrine disruptors from urban wastewater by advanced oxidation processes (AOPs): a review, Open Biotechnol. J., 10 (2016) 151–172.
[16] M. Umar, F. Roddick, L. Fan, H.A. Aziz, Application of ozone for the removal of bisphenol A from water and wastewater – a review, Chemosphere, 90 (2013) 2197–2207.
[17] M. Umar, H.A. Aziz, M.S. Yusoff, Trends in the use of Fenton, electro-Fenton and photo-Fenton for the treatment of landfill leachate, Waste Manage., 30 (2010) 2113–2121.
[18] C. Wang, H. Zhang, F. Li, L. Zhu, Degradation and mineralization of bisphenol A by mesoporous Bi_2WO_6 under simulated solar light irradiation, Environ. Sci. Technol., 44 (2010) 6843–6848.
[19] M. Ahmadi, H. Rahmani, A. Takdastan, N. Jaafarzadeh, A. Mostoufi, A novel catalytic process for degradation of bisphenol A from aqueous solutions: a synergistic effect of nano-Fe_3O_4@Alg-Fe on O_3/H_2O_2, Process Saf. Environ. Prot., 104 (2016) 413–421.
[20] L. Zhang, H. Ye. L. Zhao, L. Zhang, L. Yao, Y. Zhang, H. Li, Design isolated iron species for Fenton reaction: lyophilization beat calcination treatment, Chem. Commun., 51 (2015), doi: 10.1039/C5CC06590A.
[21] L. Chen, J. Ma, X. Li, J. Zhang, J. Fang, Y. Guan, P. Xie, Strong enhancement on Fenton oxidation by addition of hydroxylamine to accelerate the ferric and ferrous iron cycles, Environ. Sci. Technol., 45 (2011) 3925–3930.
[22] M. Rezaei, A. Nezamzadeh-Ejhieha, The ZnO-NiO nano-composite: a brief characterization, kinetic and thermodynamic study and study the *Arrhenius* model on the sulfasalazine photodegradation, Int. J. Hydrogen Energy, 45 (2020) 24749–24764.
[23] H. Derikvandi, A. Nezamzadeh-Ejhieh, Synergistic effect of p-n heterojunction, supporting and zeolite nanoparticles in enhanced photocatalytic activity of NiO and SnO_2, J. Colloid Interface Sci., 490 (2017) 314–327.
[24] N.E. Fard, R. Fazaeli, Experimental design study of RB 255 photocatalytic degradation under visible light using synthetic Ag/TiO_2 nanoparticles: optimization of experimental conditions, Iran J. Catal., 8 (2018) 133–141.
[25] P.S. Basavarajappa, S.B. Patil, N. Ganganagappa, K.R. Reddy, A.V. Raghu, C.V. Reddy, Recent progress in metal-doped TiO_2, non-metal doped/codoped TiO_2 and TiO_2 nanostructured hybrids for enhanced photocatalysis, Int. J. Hydrogen Energy, 45 (2020) 7764–7778.
[26] K. Djebli, H. Tebani, A. Abdessemed, N. Keghouche, Structural, optical and photocatalytic properties of ZnS/zeolite Y nanoparticles synthesized by γ-ray irradiation, Mater. Sci. Semicond. Process., 103 (2019) 104599, doi: 10.1016/j.mssp.2019.104599.
[27] Q. Wu, Z. Zhang, The fabrication of magnetic recyclable nitrogen modified titanium dioxide/strontium ferrite/diatomite heterojunction nanocomposite for enhanced visible-light-driven photodegradation of tetracycline, Int. J. Hydrogen Energy, 44 (2019) 8261–8272.
[28] N. Raza, W. Raza, H. Gul, K.-H. Kim, ZnO-ZnTe hierarchical superstructures as solar-light-activated photocatalysts for azo dye removal, Environ. Res., 194 (2021) 110499, doi: 10.1016/j.envres.2020.110499.
[29] M. Fazlzadeh, A. Rahmani, H.R. Nasehinia, H. Rahmani, K. Rahmani, Degradation of sulfathiazole antibiotics in aqueous solutions by using zero valent iron nanoparticles and hydrogen peroxide, Koomesh, (2016) 350–356.
[30] S. Dianat, Visible light induced photocatalytic degradation of direct red 23 and direct brown 166 by $InVO_4$-TiO_2 nanocomposite, Iran. J. Catal., 8 (2018) 121–132.
[31] M. Bordbar, Z. Sayban, A. Yeganeh-Faal, B. Khodadadi, Incorporation of Pb^{2+}, Fe^{2+} and Cd^{2+} ions in ZnO nanocatalyst for photocatalytic activity, Iran. J. Catal., 8 (2018) 113–120.
[32] S. Zarezadeh, A. Habibi-Yangjeh, M. Mousavi, S. Ghosh, Novel ZnO/Ag_3PO_4/AgI photocatalysts: preparation, characterization, and the excellent visible-light photocatalytic performances, Mater. Sci. Semicond. Process., 119 (2020) 105229, doi: 10.1016/j.mssp.2020.105229.
[33] M.L. Maya-Treviño, M. Villanueva-Rodríguez, J.L. Guzmán-Mar, L. Hinojosa-Reyesa, A. Hernández-Ramírez, Comparison of the solar photocatalytic activity of ZnO-Fe_2O_3 and ZnO-Fe^0 on 2,4-D degradation in a CPC reactor, Photochem. Photobiol. Sci., 14 (2015) 543–549.
[34] E.R. Bandala, C.A. Arancibia-Bulnes, S.L. Orozco, C.A. Estrada, Solar photoreactors comparison based on oxalic acid photocatalytic degradation, Sol. Energy, 77 (2004) 503–512.
[35] E.G. Mbonimpa, B. Vadheim, E.R. Blatchley, Continuous-flow solar UVB disinfection reactor for drinking water, Water Res., 46 (2012) 2344–2354.
[36] A. Yazdanbakhsh, A. Rahmani, M. Massoudinejad, M. Jafari, M. Dashtdar, Accelerating the solar disinfection process of water using modified compound parabolic concentrators (CPCs) mirror, Desal. Water Treat., 57 (2016) 23719–23727.

[37] A. Yazdanbakhsh, K. Rahmani, H. Rahmani, M. Sarafraz, M. Tahmasebizadeh, A. Rahmani, Inactivation of Fecal coliforms during solar and photocatalytic disinfection by zinc oxide (ZnO) nanoparticles in compound parabolic concentrators (CPCs), Iran. J. Catal., 9 (2019) 339–346.
[38] M. Ahmadi, K. Rahmani, A. Rahmani, H. Rahmani, Removal of benzotriazole by photo-Fenton like process using nano zero-valent iron: response surface methodology with a Box–Behnken design, Pol. J. Chem. Technol., 19 (2017) 104–112.
[39] M. Rezaee, Y. Yamini, S. Shariati, A. Esrafili, M. Shamsipur, Dispersive liquid–liquid microextraction combined with high-performance liquid chromatography-UV detection as a very simple, rapid and sensitive method for the determination of bisphenol A in water samples, J. Chromatogr. A, 1216 (2009) 1511–1514.
[40] L. Xu, L. Yang, E.M.J. Johansson, Y. Wang, P. Jin, Photocatalytic activity and mechanism of bisphenol A removal over TiO_{2-x}/rGO nanocomposite driven by visible light, Chem. Eng. J., 350 (2018) 1043–1055.
[41] G. Moussavi, M. Pourakbar, S. Shekoohiyan, M. Satari, The photochemical decomposition and detoxification of bisphenol A in the VUV/H_2O_2 process: degradation, mineralization, and cytotoxicity assessment, Chem. Eng. J., 331 (2018) 755–764.
[42] M. Masihpour, H. Nassehinia, A. Rahmani, Photocatalytic degradation of cefazolin over TiO_2 coated on the fixed bed under UV_C and solar, Desal. Water Treat., 184 (2020) 243–251.
[43] M. Babaahamdi-Milani, A. Nezamzadeh-Ejhieh, A comprehensive study on photocatalytic activity of supported Ni/Pb sulfide and oxide systems onto natural zeolite nanoparticles, J. Hazard. Mater., 318 (2016) 291–301.
[44] H. Derikvandi, A. Nezamzadeh-Ejhieh, A comprehensive study on electrochemical and photocatalytic activity of SnO_2-ZnO/clinoptilolite nanoparticles, J. Mol. Catal. A: Chem., 426 (2017) 158–169.
[45] A. Noruozi, A. Nezamzadeh-Ejhieh, Preparation, characterization, and investigation of the catalytic property of α-Fe_2O_3-ZnO nanoparticles in the photodegradation and mineralization of methylene blue, Chem. Phys. Lett., 752 (2020) 137587, doi: 10.1016/j.cplett.2020.137587.
[46] S. Aghdasi, M. Shokri, Photocatalytic degradation of ciprofloxacin in the presence of synthesized ZnO nanocatalyst: the effect of operational parameters, Iran. J. Catal., 6 (2016) 481–487.
[47] Y.M. Kang, M.K. Kim, K.D. Zoh, Effect of nitrate, carbonate/bicarbonate, humic acid, and H_2O_2 on the kinetics and degradation mechanism of bisphenol-A during UV photolysis, Chemosphere, 204 (2018) 148–155.
[48] B. Wang, F. Wu, P. Li, N. Deng, UV-light induced photodegradation of bisphenol A in water: kinetics and influencing factors, React. Kinet. Catal. Lett., 92 (2007) 3–9.
[49] M. Pirhashemi, A. Habibi-Yangjeh, Preparation of novel nanocomposites by deposition of Ag_2WO_4 and AgI over ZnO particles: efficient plasmonic visible-light-driven photocatalysts through a cascade mechanism, Ceram. Int., 43 (2017) 13447–13460.
[50] M. Moonsiri, P. Rangsunvigit, S. Chavadej, E. Gulari, Effects of Pt and Ag on the photocatalytic degradation of 4-chlorophenol and its by-products, Chem. Eng. J., 97 (2004) 241–248.
[51] A. Nezamzadeh-Ejhieh, S. Tavakoli-Ghinani, Effect of a nano-sized natural clinoptilolite modified by the hexadecyltrimethyl ammonium surfactant on cephalexin drug delivery, C.R. Chim., 17 (2014) 49–61.
[52] M. Mansoury, H. Godini, G. Shams Khorramabadi, Photocatalytic removal of natural organic matter from aqueous solutions using zinc oxide nanoparticles immobilized on glass, Iran. J. Health. Environ., 8 (2015) 181–190.
[53] J.M. Lee, M.S. Kim, B.W. Kim, Photodegradation of bisphenol-A with TiO_2 immobilized on the glass tubes including the UV light lamps, Water Res., 38 (2004) 3605–3613.
[54] R. Dianati Tilaki, M.A. Zazoli, J. Charati, M. Alamgholilu, E. Rostamali. Degradation of 4-chlorophenol by sunlight using catalyst of zinc oxide, J. Mazand. Univ. Med. Sci., 23 (2014) 195–201.
[55] T. Nakashima, Y. Ohko, Y. Kubota, A. Fujishima, Photocatalytic decomposition of estrogens in aquatic environment by reciprocating immersion of TiO_2-modified polytetrafluoroethylene mesh sheets, J. Photochem. Photobiol., A, 160 (2003) 115–120.
[56] R. Wang, D. Ren, S. Xia, Y. Zhang, J. Zhao, Photocatalytic degradation of bisphenol A (BPA) using immobilized TiO_2 and UV illumination in a horizontal circulating bed photocatalytic reactor (HCBPR), J. Hazard. Mater., 169 (2009) 926–932.
[57] K.V.A. Kumar, B. Lakshminarayana, T. Vinodkumar, C. Subrahmanyam, Cu-ZnO for visible light induced mineralization of bisphenol-A: impact of Cu ion doping, J. Environ. Chem. Eng., 7 (2019) 103057, doi: 10.1016/j.jece.2019.103057.
[58] J. Sharma, I.M. Mishra, V. Kumar, Degradation and mineralization of bisphenol A (BPA) in aqueous solution using advanced oxidation processes: UV/H_2O_2 and oxidation systems, J. Environ. Manage., 156 (2015) 266–275.
[59] G. Moussavi, M. Pourakbar, S. Shekoohiyan, M. Satari, The photochemical decomposition and detoxification of bisphenol A in the VUV/H_2O_2 process: degradation, mineralization, and cytotoxicity assessment, Chem. Eng. J., 331 (2018) 755–764.
[60] N. Bolong, A.F. Ismail, M.R. Salim, D. Rana, T. Matsuura, A. Tabe-Mohammadi, Negatively charged polyethersulfone hollow fiber nanofiltration membrane for the removal of bisphenol A from wastewater, Sep. Purif. Technol., 73 (2010) 92–99.
[61] D.P. Subagio, M. Srinivasan, M. Lim, T.T. Lim, Photocatalytic degradation of bisphenol-A by nitrogen-doped TiO_2 hollow sphere in a vis-LED photoreactor, Appl. Catal., B, 95 (2010) 414–422.
[62] O. Bechambi, S. Sayadi, W. Najjar, Photocatalytic degradation of bisphenol A in the presence of C-doped ZnO: effect of operational parameters and photodegradation mechanism, J. Ind. Eng. Chem., 32 (2015) 201–210.